

## Hierarchical structure of the energy landscape in the Voronoi model of dense tissue

Diogo E. P. Pinto <sup>1,2</sup>, Daniel M. Sussman <sup>3,\*</sup>, Margarida M. Telo da Gama <sup>1,2</sup> and Nuno A. M. Araújo <sup>1,2,†</sup>

<sup>1</sup>*Centro de Física Teórica e Computacional, Faculdade de Ciências, Universidade de Lisboa, 1749-016 Lisboa, Portugal*

<sup>2</sup>*Departamento de Física, Faculdade de Ciências, Universidade de Lisboa, 1749-016 Lisboa, Portugal*

<sup>3</sup>*Department of Physics, Emory University, Atlanta, 30322 Georgia, USA*



(Received 29 September 2021; accepted 10 May 2022; published 6 June 2022)

The Voronoi model is a popular tool for studying confluent living tissues. It exhibits an anomalous glassy behavior even at very low temperatures or weak active self-propulsion, and at zero temperature, the model exhibits a disordered solid structure with no evidence of a rigidity transition. Here, we investigate the properties of the energy landscape in this limit. We find that the structure of the energy landscape changes as a function of the preferred shape parameter of the cells  $p_0$ . We find two disordered solid phases that have similar structural features but differ in the ultrametricity of their energy landscapes; the crossover between these two states shares phenomenological properties with a Gardner transition. We further highlight how the metric used to calculate distances between configurations influences the ability to detect hierarchical arrangements of basins in the energy landscape.

DOI: [10.1103/PhysRevResearch.4.023187](https://doi.org/10.1103/PhysRevResearch.4.023187)

### I. INTRODUCTION

Understanding the collective behavior of cells in biological tissues has become one of the major interdisciplinary challenges of recent years, with applications ranging from wound healing to cancer treatment [1–7]. Both experimental and theoretical efforts have been crucial in understanding the properties of these tissues and the mechanisms by which they are regulated, for example, in the way that tissues can transition from rigid to flexible as the properties of individual cells are regulated [3,8–13]. Rigidity transitions are also seen in particulate systems, such as granular materials and colloidal suspensions, in which changes in particle density and temperature can lead to disordered materials in a kinetically arrested jammed or glassy state [14–16]. In living tissues, the nature and properties of the rigid states are still under debate, owing both to the explicitly nonequilibrium nature of cellular motion and the many-body interactions found in confluent tissue [3–5,8–10,17,18]. These differences raise several challenges to the generalization of ideas and methods developed in the context of well-studied particulate matter [4,5,8,17,18].

Several models have been proposed to understand the collective behavior of cellular systems, from single-particle descriptions to density field models [19–24]. The Voronoi model represents an epithelial confluent tissue as a space-filling polygonal tiling, where each positional degree of

freedom corresponds to a cell whose shape is obtained by an instantaneous Voronoi tessellation [19–22,25–27]. The dynamics is controlled by an energy functional that is quadratic in the area and perimeter of each cell, and the mechanical properties of the tissue can be either solidlike or fluidlike depending on the temperature and a shape parameter  $p_0$ , which quantifies the target shape of the individual cells [25].

A distinguishing aspect of this transition is that it depends significantly on  $p_0$  [3,20,25]. Recent experimental results show that the fluidity of the tissue correlates directly with cell shape [13]. This suggests that, even if noise (e.g., activity) is present, both the dynamics of cells and mechanics of the tissue are strongly dependent on the properties of the energy landscape. At zero temperature (i.e., in the absence of cellular activity), it has been argued that the Voronoi model always possesses a finite shear modulus [28]. This is in sharp contrast with particulate systems, in which a zero-temperature rigidity transition can be observed by changing the density [14–16,29–32]. The particulate jamming transition is typically interpreted in the context of constraint counting, in which the transition occurs when the number of independent particle-particle contacts equals the number of degrees of freedom [33,34]. As described below, the two-dimensional (2D) Voronoi model is always at this point of marginal stability [28], and thus, such an analysis is insufficient. It has been proposed instead that energetic rigidity, in which not only simple constraints but also residual stresses play a controlling role [17,18,35,36], is a better framework for understanding Voronoi model rigidity [36].

Here, we explore this unusual athermal regime of the Voronoi model and show that, even in the absence of a zero-temperature rigidity transition, there is a profound change in the statistics of the energy landscape. By considering this limit, we remove the contribution of activity (or temperature) and focus on the properties of the landscape. In glasses, the energy landscape is characterized by multiple deep wells or

\*daniel.m.sussman@emory.edu

†Corresponding author: nmaraujo@fc.ul.pt

basins, which give rise to their metastability [29,31]. Near the Gardner transition, each basin is divided into smaller subbasins in a hierarchical structure with an ultrametric property. The ultrametric state is characterized by energy minima forming a treelike structure in phase space where minima within a given subbasin are much closer to one another than they are to minima in any other subbasin [29,31]. We find evidence for a transition to such a hierarchical arrangement of basins in the energy landscape, suggesting two different phases of a disordered solid [37–40]. This is consistent with a Gardner phenomenology [29,31]; this has implications for the mechanical and dynamical properties of the system, as has been studied in multiple experimental and computational systems [37–42].

## II. MODEL

We model the confluent tissue as a monolayer of  $N$  cells [19,20,25] in a square domain of side length  $L$  with periodic boundary conditions. Each cell  $i$  is represented by its center  $\mathbf{r}_i$  with a shape given by an instantaneous Voronoi tessellation of the space. We choose the unit of length to be given by the square root of the average area of all the cells. We can then write a dimensionless version of the contribution of each cell to the energy functional as [17,21,22,43]

$$e_i = k_A(a_i - 1)^2 + (p_i - p_0)^2. \quad (1)$$

Here,  $a_i$  and  $p_i$  are the dimensionless area and perimeter of cell  $i$ ,  $p_0$  is the shape parameter, and  $k_A$  represents the ratio between the relative stiffness of the area and perimeter elasticity of the cell. Biologically, the first term models cellular incompressibility and the resistance of the cellular monolayer to height fluctuations; the second term models the competition between active contractility of the actomyosin subcellular cortex and the effective cell membrane tension due to cell-cell adhesion and cortical tension.

For each set of parameters, we start with  $N$  cells distributed at random positions. The configuration is then minimized using the FIRE algorithm [44,45], which we halt when the maximum net force on each cell is  $<10^{-12}$ . Due to numerical constraints, we consider  $p_0 \leq 3.85$  [28]. Further details of the simulations can be found below in the Methods section.

To probe the structure of the energy landscape, we start from an initial configuration that corresponds to a local minimum and perturb it to find new stable configurations. Our goal is not to completely explore the energy landscape but rather to characterize the arrangement of locally stable minima. In our primary perturbation protocol, we displace the position of each cell according to the vector  $\vec{P}_\varepsilon = [X_0, X_1, \dots, X_{2N-1}]$ , where  $N$  is the number of cells,  $X_{2i} = \varepsilon \cos(\theta_i)$  is the perturbation to cell  $i$  along the  $x$  axis,  $X_{2i+1} = \varepsilon \sin(\theta_i)$  is that along the  $y$  axis, and  $\theta_i$  is a random angle uniformly distributed between 0 and  $2\pi$ . We considered a random length  $\varepsilon$  drawn from a uniform distribution between 0 and  $\varepsilon_{\max}$ ; thus, each cell will move a random displacement to guarantee the possibility of visiting minima in the same and different top-level basins. The norm of the perturbation vector is  $|\vec{P}_\varepsilon| = P_\varepsilon = \varepsilon\sqrt{N}$ . After the perturbation, we subtract the global translation of the tissue and then let the tissue relax to a new minimum

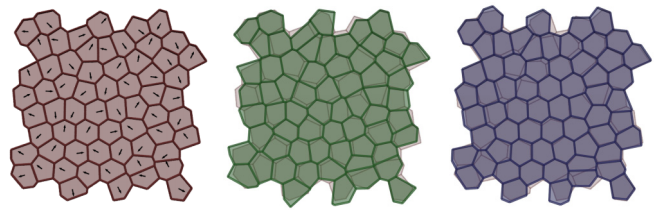


FIG. 1. Representation of the perturbation protocol. (Left) Original minimized configuration (red) with the perturbation vectors. (Middle) Minimized (red) and perturbed (green) configurations. (Right) Minimized configurations before (red) and after (blue) perturbation.

(Fig. 1). Details of alternate perturb-and-minimize schemes can be found in the Supplemental Material [46], where we show that our results are not qualitatively sensitive to these details.

## III. RESULTS

There has been a sustained effort to characterize the structure of the energy landscape and relate it to material properties [38,47]. One approach is through quantifying how much a given minimized configuration changes after perturbations [40]. A metric can be used to measure the distance, in configurational space, between two different configurations and reconstruct the energy landscape to measure its properties, given that sufficient minima have been probed. Recent studies have explored how the Voronoi model exhibits unique properties when compared with other glassy systems [27,48,49], and thus, we apply a similar approach here. We will be exploring different metrics to characterize distances between minima. First, we consider the contact metric (denoted by the superscript  $X$ ) discussed in Refs. [38–40]:

$$d^X(a, b) = \sqrt{\sum_{ij} (\vec{C}_{ij}^a - \vec{C}_{ij}^b)^2}, \quad (2)$$

where  $d^X(a, b)$  is the distance between configuration  $a$  and  $b$ , and  $\vec{C}_{ij}^a$  is the 2D contact vector between two cells, where each component  $C_{ij,x}^a = x_i^a - x_j^a$  is the distance along the respective axis between cells  $i$  and  $j$  if those cells share an edge, and  $\vec{C}_{ij}^a = \vec{0}$  otherwise.

Figure 2 shows how the normalized distance to the original minimum, using the contact metric, scales with the norm of the perturbation vector applied, computed after subtracting the global translation, where  $|a| = \sqrt{\sum_{ij} (C_a^{ij})^2}$  corresponds to  $d^X(a, b)$  for which  $C_b^{ij} = 0$ . Here,  $a$  was fixed and corresponds to the initial configuration, while  $b$  is the minimum after the perturbation. We observe that the distance to the original minimum scales approximately linearly with the norm of the perturbation. Furthermore, as in Ref. [40], by rescaling the perturbation by  $\sqrt{N}$ , we observe a collapse of the curves for different system sizes. Thus,  $d^X(a, b) \sim \sqrt{N}$ , and we choose  $\varepsilon_{\max} = 0.5\sqrt{N}$  for all  $p_0$ , which is large enough so that the perturbed configuration does not always relax to the initial minimum but small enough that nearby minima are accessible. This protocol, although simple, is quite effective at biasing the

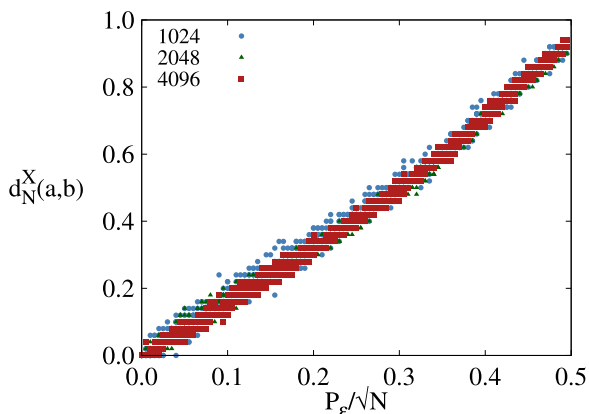


FIG. 2. Scatter plot of the distribution of normalized metric distance to the original minimum for different norms of the perturbation vector, using the contact metric. The metric distance defined in Eq. (2) is normalized by  $\sqrt{|a||b|}$ , where  $|a| = d(a, 0)$ . For  $p_0 = 3.81$ , all sizes collapse onto the same curve when using this scaling; thus, we choose  $\epsilon_{\max} = 0.5\sqrt{N}$ .

configurations to visit only nearby minima. To explore a wider range, different probing techniques should be used [47].

A Gardner phase is characterized by an ultrametric phase space consisting of a treelike structure, where minima within a given subbasin are all much closer to one another than to minima in any other subbasin. This property is codified by an ultrametric inequality,  $d^X(a, c) \leq \max[d^X(a, b), d^X(b, c)]$ , where  $a, b$ , and  $c$  are three different configurations in phase space, and  $d^X(a, b)$  is the distance between configurations. To verify if the properties of the tissue are consistent with a Gardner phase, we compute how close the metric is to being ultrametric. To do so, we first find the subdominant ultrametric  $d^<(a, b)$ , i.e., the ultrametric that is closest to  $d^X(a, b)$  itself. The subdominant ultrametric can

be found by first computing the distances in the minimum spanning tree of the space of minima [50]. Then for each pair of minima  $a$  and  $b$ , we compute the path between them in the minimum spanning tree and define  $d^<(a, b)$  as the largest distance between two neighboring minima along the path [51].

Figure 3 depicts matrices where the color corresponds to the distance between minima, for all pairs of minima found for  $p_0 = 3.75$  and  $3.83$ . These matrices were constructed for  $10^3$  minima obtained for a tissue of 4096 cells. Each element of the matrix corresponds to the distance between two minima,  $a$  and  $b$ , given by Eq. (2). The distances are all sorted using the single-linkage clustering algorithm on the metric of the fully minimized systems, which groups them sequentially based on their relative distance [52]. The colors represent different distances. In white are the minima that are closest to each other. We find groups of minima that are all at this minimum distance, forming a white region that corresponds to subbasins. The matrices do not show any substantial visual change with  $p_0$ .

Having found  $d^<(a, b)$ , we finally calculate the generalized distance between the metric and the subdominant ultrametric using

$$D^X = \sqrt{\langle [d^X(a, b) - d^<(a, b)]^2 \rangle}, \tag{3}$$

where  $\langle \cdot \rangle$  denotes the average over all configuration pairs  $a$  and  $b$ . If  $D^X = 0$ , then the energy landscape is ultrametric, while  $D^X > 0$  quantifies how far it is from ultrametricity. In the inset of Fig. 3, we show that  $D^X$  depends strongly on  $N$ . In the main plot, we rescale  $D^X/\sqrt{N}$  and obtain a reasonable collapse of the data. Since the typical distance between minima and the distance to ultrametricity both scale with  $\sqrt{N}$ , the landscape with this contact metric is not ultrametric in the thermodynamic limit [40].

Using distances based on the contact vectors suggests that the landscape of the Voronoi model is not ultrametric, but does the choice of metric itself influence this result? In systems

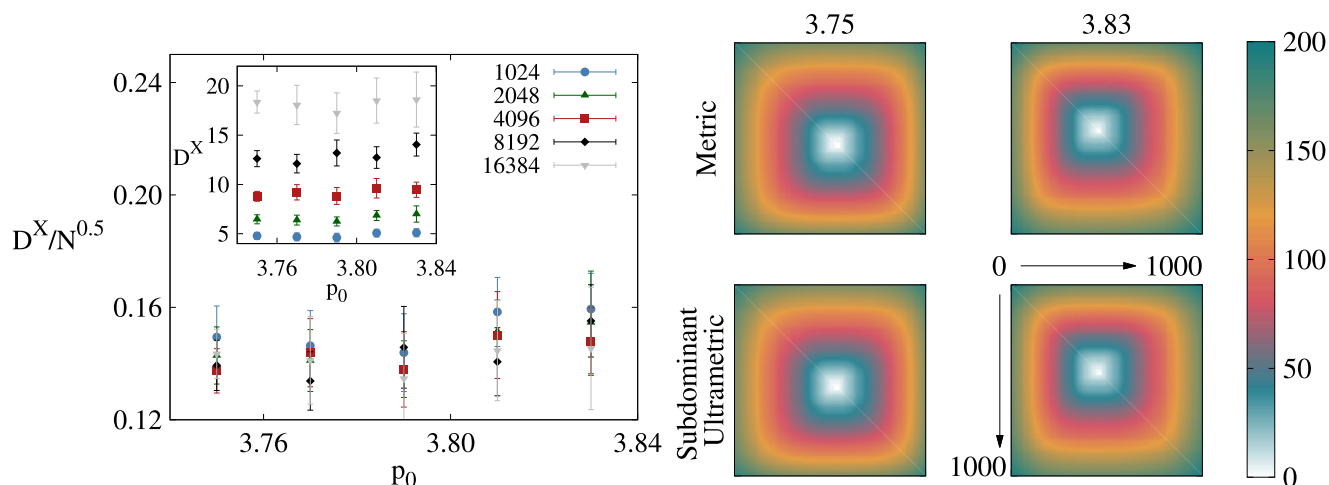


FIG. 3. (Left) Normalized generalized distance to ultrametricity as measured using the contact vector metric  $D^X/\sqrt{N}$  as a function of  $p_0$ , for  $N = 1024, 2048, 4096, 8192$ , and  $16384$ . The inset shows the same results without the scaling. These are averages of 10 initial configurations subject to 100 perturbations and minimizations each. (Right) A schematic representation of the distances between minima according to the contact metric  $d^X(a, b)$  and the subdominant ultrametric constructed from it using a minimum spanning tree. Matrices corresponding to  $N = 4096$  and  $p_0 = 3.75$  and  $3.83$  are shown, where the different distances are grouped using a single-linkage clustering algorithm which clusters the minima sequentially by distance.

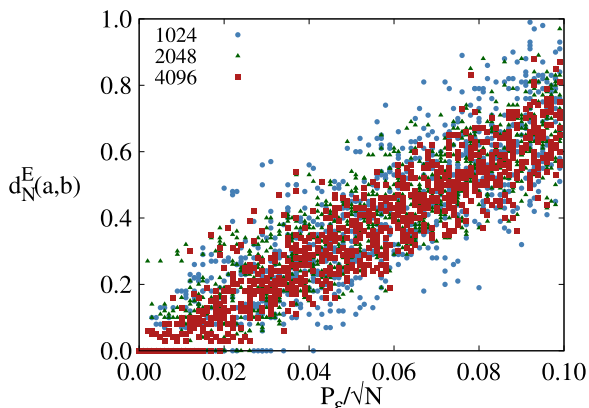


FIG. 4. Scatter plot of the distribution of normalized metric distance to the original minimum for different norms of the perturbation vector, using the energy metric. The metric distance defined in Eq. (2) is normalized by  $\sqrt{|a||b|}$ , where  $|a| = d(a, 0)$ . For  $p_0 = 3.81$ , all sizes collapse onto the same curve when using this scaling; thus, we choose  $\epsilon_{\max} = 0.1\sqrt{N}$ .

composed of soft or hard spheres, the interactions are usually pairwise and depend explicitly on the position of the particles. Thus, metrics based on the number of contacts are expected to adequately characterize the structure of the energy landscape [40]. In the Voronoi model, the number of contacts per cell does not change significantly even as the tissue rigidity changes substantially [18,36]. We further note that the energy functional in Eq. (1) is a simple collection of harmonic springs, in a coordinate basis of shape space rather than in the basis of the positional degrees of freedom generating the shapes. We propose a metric based on the contribution of each cell  $i$  to the total energy of the tissue  $e_i$ . We take the same form for the metric as Eq. (2) but where  $\tilde{C}_{ij}^a \rightarrow C_{ij}^a = e_i^a - e_j^a$  if  $i$  and  $j$  are neighbors and zero otherwise. We call this metric

the energy metric  $d^E(a, b)$ . We adopt the same perturb-and-minimize protocol as before, using  $\epsilon_{\max} = 0.1\sqrt{N}$  for all  $p_0$  (Fig. 4). In the Supplemental Material [46], we show that the results using the contact metric remain qualitatively the same using the new  $\epsilon_{\max}$ . The energy metric also scales with system size  $d^E(a, b) \sim \sqrt{N}$  since it depends on the total number of cell-cell contacts. We observe in the inset of Fig. 5 that, for the energy metric, the distance to ultrametricity ( $D^E$ ) does not scale with  $N$  and decreases with  $p_0$  (inset of Fig. 5). Since the distance between minima scales as  $d^E(a, b) \sim \sqrt{N}$ , while the generalized distance does not depend on the system size, this suggests that the system does become ultrametric in the thermodynamic limit:  $D^E/d^E(a, b) \sim 1/\sqrt{N}$ .

In the case of the contact metric, the calculated values are already normalized since we increase the box size with  $N$ , while the typical cell size is fixed. For the energy metric, this is no longer the case. Thus, to properly compare the system properties at different  $p_0$  (since  $\langle E_i \rangle$  varies with  $p_0$ ), we consider a normalized version of the energy metric:  $d_N^E(a, b) = d^E(a, b)/\sqrt{|a||b|}$ , for which the typical distance between configurations does not depend on either  $p_0$  or  $N$ . Figure 5 depicts matrices where the color corresponds to the distance between minima, for all pairs of minima found for  $p_0 = 3.75$  and 3.83. These matrices were constructed for  $10^3$  minima obtained for a tissue of 4096 cells. Each element of the matrix corresponds to the distance between two minima,  $a$  and  $b$ , using  $d_N^E(a, b)$ . From this representation, we can already observe changes in the structure of the energy landscape. As  $p_0$  increases, the color gradient is less smooth, and the boxes corresponding to the different subbasins become sharper. It is also observed that more minima fall into the same subbasin. These properties suggest that, when the value of  $p_0$  decreases, the structure of the energy landscape becomes more hierarchical [40]. This is in contrast with the matrices obtained using  $d^X(a, b)$ , which do not show any substantial visual change with  $p_0$ .

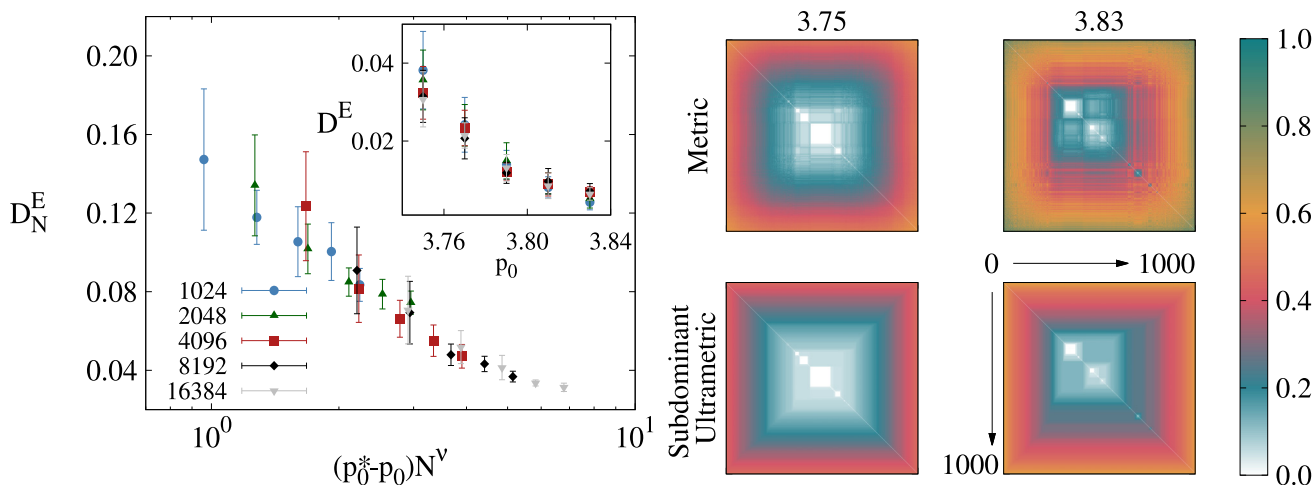


FIG. 5. (Left) Normalized generalized distance to ultrametricity as measured using the normalized energy metric  $D_N^E$  as a function of  $(p_0^* - p_0)N^\nu$ , for  $N = 1024, 2048, 4096, 8192,$  and  $16384$ ,  $p_0^* = 3.89 \pm 0.01$ , and  $\nu = 0.40 \pm 0.01$ . The inset shows the generalized distance to ultrametricity  $D^E$  as a function of  $p_0$ . These are averages of 10 initial configurations subject to 100 perturbations and minimizations each. (Right) Schematic matrix representation of the distances between minima according to the normalized energy metric  $d_N^E(a, b)$  and its subdominant ultrametric. Matrices corresponding to  $N = 4096$  and  $p_0 = 3.75$  and 3.83 are shown, where the different distances are grouped using a single-linkage clustering algorithm which clusters the minima sequentially by distance.

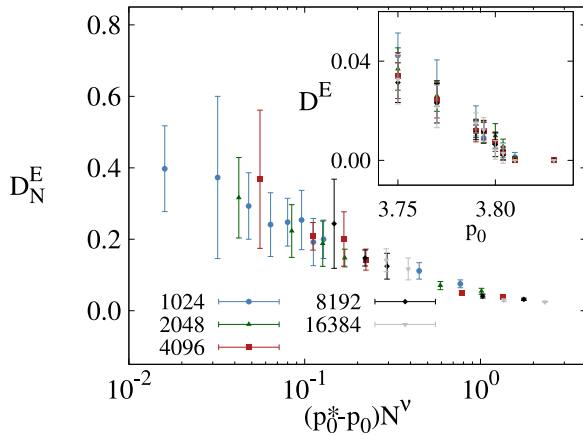


FIG. 6. A plot as in Fig. 5 but for  $k_A = 0$ , highlighting the similar scaling in the two cases. Here, we use  $p_0^* = 3.798 \pm 0.001$  and  $\nu = 0.40 \pm 0.01$ . These are averages of 10 initial configurations subject to 100 perturbations and minimizations each

We also compute the generalized distance to ultrametricity with  $d_N^E$ . Again, we see that ultrametricity is approached with increasing system size. Furthermore, with the scaling shown in the main panel of Fig. 5, we can collapse the different curves. The values of  $p_0^*$  and  $\nu$  were chosen such that we obtain the best collapse. Recent work in particulate systems has interpreted a similar scaling as a distance to jamming [30,40]. This suggests not only that the Voronoi model has an ultrametric structure in the thermodynamic limit but that there may be a transition between two different solid phases. Previously, it was shown that the athermal Voronoi model did not have a rigidity transition [28]. Nevertheless, we show that there is a clear difference between the energy landscape for low and high  $p_0$ : At low  $p_0$ , the glass state is characterized by large residual stresses and an ultrametric energy landscape, and at high  $p_0$ , the energy landscape is not ultrametric. We find that this change occurs for preferred shape parameters in the range  $p_0 = 3.75 - 3.85$ , which is close to where the zero-temperature shear modulus changes markedly [28] and where the dynamics at finite temperature changes in character [25,27,48].

As  $p_0$  increases, fewer subbasins are found inside each basin (as represented by the different unconnected clusters in Fig. 5), suggesting that the energy landscape flattens. We explore this flattening by studying the behavior of the model as  $k_A$  is varied. In the limit  $k_A = 0$ , the Voronoi model is no longer marginally constrained, and it acquires a residual-stress-based rigidity transition as a function of  $p_0$  at  $T = 0$  [28]. As shown in Fig. 6, for  $p_0 < 3.79$ , we find that the tissue is rigid, and the energy landscape is ultrametric. For slightly larger  $p_0$ , the energy landscape deviates from ultrametricity. In this regime, the energy landscape consists of a mixture of hierarchical basins and several nearly flat basins, and so, in many cases, small perturbations will not drive the system to a different minimum. In the Supplemental Material [46], we use a simple technique to estimate the transition from the solid to the fluid phase. Using the fraction of configurations with zero energy, we estimate a transition point around  $p_0^* = 3.8022 \pm 0.0001$ , while in Fig. 6,  $p_0^* = 3.798 \pm 0.001$  seems

to be a more appropriate value to collapse the data. We used  $\nu = 0.40 \pm 0.01$ , which was the best value for the collapse. More simulations would be needed to conclude whether a new solid phase at  $k_A = 0$  exists before the fluid phase or if the observations are finite-sized effects and both transitions actually coincide. We stress that this approach signals a possible transition through the observed changes of the energy landscape. Nonetheless, previous studies of the mechanical response of the model support the existence of such a transition [28]. For  $p_0 > 3.8$ , the energy landscape is flat, characteristic of a fluidlike tissue. For any  $k_A > 0$ , different energy minima are found for all  $p_0$ , consistent with previous work showing a finite shear modulus for the whole range of model parameters investigated [28]. Recent studies with the thermal 2D Voronoi model also suggest a change in the energy landscape close to  $p_0 \approx 3.81$  [48].

#### IV. CONCLUSIONS

In summary, we have found indications of a hierarchical structure of the energy landscape in a model of dense biological tissue whose zero-temperature rigidity is quite different from that of constraint-based particulate systems. Strikingly, we find that the choice of metric to characterize distances between minima is crucial: Defining distance based on changes in neighboring contact vectors vs contributions to the energy give qualitatively different interpretations of the structure of the energy landscape. In particulate systems, the contact vectors enter explicitly in the relevant energy functional, i.e., the energy of a soft harmonic repulsion or a Lennard-Jones interaction is a simple function of the contact vector between interacting particles. In Voronoi models, the energy cannot be decomposed into independent pairwise contributions, which we speculate is the reason that choosing a distance metric based on the total energy associated with each degree of freedom is required to uncover the hierarchical structure of the landscape. We further speculate that this may point more generally to the importance of the choice of metric for systems in which many-body interactions dominate over pairwise ones; for example, previous studies have shown that this is the case in compressed high-density systems of soft particles, like microgels or foams [53]. In this paper, we suggest that, under the proper choice of metric, ultrametricity should emerge in those systems, as observed for other glassy/jammed materials [40]. Authors of recent studies found that the Voronoi model has a unique glassy behavior inside the rigid phase [27,49]. The structure of the energy landscape can provide a deeper link between this model and other glassy systems; thus, future researchers could aim to relate these tissuelike systems to particulate ones [38,40]. This could be done by establishing a relation between the effects of  $p_0$  in the Voronoi model and pressure in particulate systems. Since both exhibit an ultrametric landscape, this could allow a generalization of glassy physics [15,16,29].

#### V. METHODS

To simulate the tissue we use cellGPU [45] and initialize  $N$  cells distributed randomly in a square periodic box of linear

size  $\sqrt{N}$  in units of  $\sqrt{A}$ . We consider a monodisperse system with  $\bar{A} = 1$ .

After initialization, the tissue is relaxed using a FIRE minimization algorithm [44]. This relaxation algorithm moves the cell centers at each step to minimize the energy, described by the functional form given in Eq. (1). The algorithm uses the standard molecular dynamics equations (with velocity Verlet integration) and two adaptive quantities, the time-step  $\Delta t$  and  $\alpha$ , the latter to adjust the integration step and the former to control the velocities. During the relaxation, when an uphill in the energy landscape is found, both decrease to minimize the amount of time spent there and then increase again when a downhill is encountered. For our simulations, we have chosen  $\Delta t_{\min} = 0.001$ ,  $\Delta t_{\max} = 0.1$ , and  $\alpha_{\text{start}} = 0.99$ . We have tested other values and have found that they do not affect substan-

tially the minimization procedure. Thus, they were kept the same in all the simulations. The minimization is halted once the maximum force on all cells is  $< 10^{-12}$  in natural units (see previous section). Due to numerical constraints, we consider  $p_0 \leq 3.85$  since it has been shown for athermal systems that, above this value, configurations with multifold vertices are obtained which lead to numerical instabilities in the minimization protocol [28].

#### ACKNOWLEDGMENTS

The authors acknowledge financial support from the Portuguese Foundation for Science and Technology (FCT) under Contracts No. PTDC/FIS-MAC/28146/2017 (LISBOA-01-0145-FEDER-028146), No. UIDB/00618/2020, No. UIDP/00618/2020, and No. SFRH/BD/131158/2017.

- 
- [1] K. Ghosh and D. E. Ingber, Micromechanical control of cell and tissue development: Implications for tissue engineering, *Adv. Drug Deliv. Rev.* **59**, 1306 (2007).
- [2] N. S. Gov, Traction forces during collective cell motion, *HSFP J.* **3**, 223 (2009).
- [3] J.-A. Park, J. H. Kim, D. Bi, J. A. Mitchel, N. T. Qazvini, K. Tantisira, C. Y. Park, M. McGill, S.-H. Kim, B. Gweon *et al.*, Unjamming and cell shape in the asthmatic airway epithelium, *Nat. Mater.* **14**, 1040 (2015).
- [4] D. T. Tambe, C. C. Hardin, T. E. Angelini, K. Rajendran, C. Y. Park, X. Serra-Picamal, E. H. Zhou, M. H. Zaman, J. P. Butler, D. A. Weitz *et al.*, Collective cell guidance by cooperative intercellular forces, *Nat. Mater.* **10**, 469 (2011).
- [5] C. Pérez-González, R. Alert, C. Blanch-Mercader, M. Gómez-González, T. Kolodziej, E. Bazellieres, J. Casademunt, and X. Trepat, Active wetting of epithelial tissues, *Nat. Phys.* **15**, 79 (2019).
- [6] R. Sunyer, V. Conte, J. Escribano, A. Elosegui-Artola, A. Labernadie, L. Valon, D. Navajas, J. M. García-Aznar, J. J. Muñoz, P. Roca-Cusachs *et al.*, Collective cell durotaxis emerges from long-range intercellular force transmission, *Science* **353**, 1157 (2016).
- [7] B. Szabó, G. J. Szöllösi, B. Gönci, Z. Jurányi, D. Selmeczi, and T. Vicsek, Phase transition in the collective migration of tissue cells: Experiment and model, *Phys. Rev. E* **74**, 061908 (2006).
- [8] T. E. Angelini, E. Hannezo, X. Trepat, M. Marquez, J. J. Fredberg, and D. A. Weitz, Glass-like dynamics of collective cell migration, *Proc. Natl. Acad. Sci. USA* **108**, 4714 (2011).
- [9] S. Garcia, E. Hannezo, J. Elgeti, J.-F. Joanny, P. Silberzan, and N. S. Gov, Physics of active jamming during collective cellular motion in a monolayer, *Proc. Natl. Acad. Sci. USA* **112**, 15315 (2015).
- [10] E.-M. Schötz, M. Lanio, J. A. Talbot, and M. L. Manning, Glassy dynamics in three-dimensional embryonic tissues, *J. R. Soc. Interface* **10**, 20130726 (2013).
- [11] A. Mongera, P. Rowghanian, H. J. Gustafson, E. Shelton, D. A. Kealhofer, E. K. Carn, F. Serwane, A. A. Lucio, J. Giammona, and O. Campàs, A fluid-to-solid jamming transition underlies vertebrate body axis elongation, *Nature (London)* **561**, 401 (2018).
- [12] S. Grosser, J. Lippoldt, L. Oswald, M. Merkel, D. M. Sussman, F. Renner, P. Gottheil, E. W. Morawetz, T. Fuhs, X. Xie *et al.*, Cell and Nucleus Shape as an Indicator of Tissue Fluidity in Carcinoma, *Phys. Rev. X* **11**, 011033 (2021).
- [13] J. Devany, D. M. Sussman, T. Yamamoto, M. L. Manning, and M. L. Gardel, Cell cycle-dependent active stress drives epithelia remodeling, *Proc. Natl. Acad. Sci. USA* **118**, e1917853118 (2021).
- [14] K. Binder and A. P. Young, Spin glasses: Experimental facts, theoretical concepts, and open questions, *Rev. Mod. Phys.* **58**, 801 (1986).
- [15] L. Berthier and G. Biroli, Theoretical perspective on the glass transition and amorphous materials, *Rev. Mod. Phys.* **83**, 587 (2011).
- [16] L. M. C. Janssen, Active glasses, *J. Phys.: Condens. Matter* **31**, 503002 (2019).
- [17] M. Merkel and M. L. Manning, A geometrically controlled rigidity transition in a model for confluent 3D tissues, *New J. Phys.* **20**, 022002 (2018).
- [18] M. Merkel, K. Baumgarten, B. P. Tighe, and M. L. Manning, A minimal-length approach unifies rigidity in underconstrained materials, *Proc. Natl. Acad. Sci. USA* **116**, 6560 (2019).
- [19] D. Bi, J. H. Lopez, J. M. Schwarz, and M. L. Manning, Energy barriers and cell migration in densely packed tissues, *Soft Matter* **10**, 1885 (2014).
- [20] D. Bi, J. H. Lopez, J. M. Schwarz, and M. L. Manning, A density-independent rigidity transition in biological tissues, *Nat. Phys.* **11**, 1074 (2015).
- [21] R. Farhadifar, J.-C. Röper, B. Aigouy, S. Eaton, and F. Jü, The influence of cell mechanics, cell-cell interactions, and proliferation on epithelial packing, *Curr. Biol.* **17**, 2095 (2007).
- [22] A. G. Fletcher, M. Osterfield, R. E. Baker, and S. Y. Shvartsman, Vertex models of epithelial morphogenesis, *Biophys. J.* **106**, 2291 (2014).
- [23] B. A. Camley and W.-J. Rappel, Physical models of collective cell motility: From cell to tissue, *J. Phys. D: Appl. Phys.* **50**, 113002 (2017).
- [24] A. J. Kabla, Collective cell migration: Leadership, invasion and segregation, *J. R. Soc. Interface* **9**, 3268 (2012).

- [25] D. Bi, X. Yang, M. C. Marchetti, and M. L. Manning, Motility-Driven Glass and Jamming Transitions in Biological Tissues, *Phys. Rev. X* **6**, 021011 (2016).
- [26] S. Kaliman, C. Jayachandran, F. Rehfeldt, and A. Smith, Limits of applicability of the Voronoi tessellation determined by centers of cell nuclei to epithelium morphology, *Front. Psychol.* **7** (2016).
- [27] D. M. Sussman, M. Paoluzzi, M. C. Marchetti, and M. L. Manning, Anomalous glassy dynamics in simple models of dense biological tissue, *Europhys. Lett.* **121**, 36001 (2018).
- [28] D. M. Sussman and M. Merkel, No unjamming transition in a Voronoi model of biological tissue, *Soft Matter* **14**, 3397 (2018).
- [29] G. Parisi and F. Zamponi, Mean-field theory of hard sphere glasses and jamming, *Rev. Mod. Phys.* **82**, 789 (2010).
- [30] C. P. Goodrich, A. J. Liu, and S. R. Nagel, Finite-Size Scaling at the Jamming Transition, *Phys. Rev. Lett.* **109**, 095704 (2012).
- [31] P. Charbonneau, J. Kurchan, G. Parisi, P. Urbani, and F. Zamponi, Glass and jamming transitions: From exact results to finite-dimensional descriptions, *Annu. Rev. Condens. Matter Phys.* **8**, 265 (2017).
- [32] A. Baule, F. Morone, H. J. Herrmann, and H. A. Makse, Edwards statistical mechanics for jammed granular matter, *Rev. Mod. Phys.* **90**, 015006 (2018).
- [33] T. C. Lubensky, C. L. Kane, X. Mao, A. Souslov, and K. Sun, Phonons and elasticity in critically coordinated lattices, *Rep. Prog. Phys.* **78**, 073901 (2015).
- [34] S. Franz, A. Sclocchi, and P. Urbani, Critical Jammed Phase of the Linear Perceptron, *Phys. Rev. Lett.* **123**, 115702 (2019).
- [35] L. Yan and D. Bi, Multicellular Rosettes Drive Fluid-solid Transition in Epithelial Tissues, *Phys. Rev. X* **9**, 011029 (2019).
- [36] O. K. Damavandi, V. F. Hagh, C. D. Santangelo, and M. L. Manning, Energetic rigidity I: A unifying theory of mechanical stability, *Phys. Rev. E* **105**, 025003 (2022).
- [37] P. Charbonneau, Y. Jin, G. Parisi, C. Rainone, B. Seoane, and F. Zamponi, Numerical detection of the gardner transition in a mean-field glass former, *Phys. Rev. E* **92**, 012316 (2015).
- [38] Q. Liao and L. Berthier, Hierarchical Landscape of Hard Disk Glasses, *Phys. Rev. X* **9**, 011049 (2019).
- [39] C. Artiago, P. Baldan, and G. Parisi, Exploratory study of the glassy landscape near jamming, *Phys. Rev. E* **101**, 052605 (2020).
- [40] R. C. Dennis and E. I. Corwin, Jamming Energy Landscape is Hierarchical and Ultrametric, *Phys. Rev. Lett.* **124**, 078002 (2020).
- [41] A. Seguin and O. Dauchot, Experimental Evidence of the Gardner Phase in a Granular Glass, *Phys. Rev. Lett.* **117**, 228001 (2016).
- [42] C. Scalliet, L. Berthier, and F. Zamponi, Absence of Marginal Stability in a Structural Glass, *Phys. Rev. Lett.* **119**, 205501 (2017).
- [43] E. Teomy, D. A. Kessler, and H. Levine, Confluent and nonconfluent phases in a model of cell tissue, *Phys. Rev. E* **98**, 042418 (2018).
- [44] E. Bitzek, P. Koskinen, F. Gähler, M. Moseler, and P. Gumbsch, Structural Relaxation Made Simple, *Phys. Rev. Lett.* **97**, 170201 (2006).
- [45] D. M. Sussman, CELLGPU: Massively parallel simulations of dynamic vertex models, *Comput. Phys. Commun.* **219**, 400 (2017).
- [46] See Supplemental Material at <http://link.aps.org/supplemental/10.1103/PhysRevResearch.4.023187> for additional information regarding the results comparing different  $k_A$  and the estimation of the rigid to fluid transition with  $k_A = 0$ .
- [47] B. Doliwa and A. Heuer, Hopping in a supercooled Lennard-Jones liquid: Metabasins, waiting time distribution, and diffusion, *Phys. Rev. E* **67**, 030501(R) (2003).
- [48] Y.-W. Li, Leon Loh Yeong Wei, M. Paoluzzi, and M. P. Ciamarra, Softness, anomalous dynamics, and fractal-like energy landscape in model cell tissues, *Phys. Rev. E* **103**, 022607 (2021).
- [49] Y. Zheng, Y.-W. Li, and M. P. Ciamarra, Hyperuniformity and density fluctuations at a rigidity transition in a model of biological tissues, *Soft Matter* **16**, 5942 (2020).
- [50] J. B. Kruskal, On the shortest spanning subtree of a graph and the traveling salesman problem, *Proc. Am. Math. Soc.* **7**, 48 (1956).
- [51] R. Rammal, J. Angles d'Auriac, and B. Doucot, On the degree of ultrametricity, *J. Phys. Lett.* **46**, 945 (1985).
- [52] F. Murtagh, A survey of recent advances in hierarchical clustering algorithms, *Comput. J.* **26**, 354 (1983).
- [53] C. N. Likos, Effective interactions in soft condensed matter physics, *Phys. Rep.* **348**, 267 (2001).